Adaptive in-cylinder pressure model for spark ignition engine control

Benjamín Pla, Joaquin De La Morena, Pau Bares, Irina Jiménez

CMT-Motores Termicos, Universitat Politecnica de Valencia, Camino de Vera s/n, E-46022 Valencia, Spain

Abstract

In-cylinder pressure is the most important variable to analyze the combustion process in internal combustion engines, and can be used used as feedback signal for closed-loop combustion control and diagnostics. However, pressure sensors are still affected by challenges such as durability and cost, which prevent their use in mass-production vehicles. Therefore, this work presents a model-based approach to estimate the in-cylinder pressure by means of the combination of a control oriented model and information from the set of sensors available in current production engines for automotive applications. Pressure peak location of each cylinder is estimated through the knock sensor signal, and used as feedback to improve the model. An extended Kalman filter is used to adapt the model to the information from the knock sensor signal. The adaptive model is implemented in a four cylinder light-duty engine and compared with the open loop model, ensuring a continuous estimation of in-cylinder pressure signal, and an improvement for the estimation of different cycle by cycle combustion parameters and cylinder to cylinder variations. Finally, the proposed approach is applied with different fuels showing that the proposed method can be applied independently on the fuel used.

Keywords: Combustion model, knock sensor, SI engine, In-cylinder pressure model, combustion control

1. Introduction

Traditionally, Internal Combustion Engines (ICE) use open-loop (OL) maps to control variables such as spark advance (SA), or variable valve timing (VVT). The OL map approach is not flexible enough to handle real engine behavior, as aging or transients conditions [1].

Closed-loop (CL) control is an effective method to cope the disadvantages of OL. The combustion phasing can be estimated from the in-cylinder pressure with a heat release analysis [2]. The SA control target is to center the combustion in the maximum efficiency point for a given operating condition [3]. A widely used method to evaluate combustion efficiency is through the indicated mean effective pressure (IMEP), which is calculated from the in-cylinder pressure trace. Many studies have applied extremum seeking (ES) methods for combustion optimization, thus the optimal SA is calibrated in real-time [4]. Other works employ on-board learning algorithms for real-time combustion control, in [5] a scheme with two layers is proposed, in which the target of the crank angle position where 50% of the heat is released (CA50) is achieved by controlling the SA through a combination of feed forward / feed back controller and a look-up table on-line calibrated. Moreover, a SA knock constrained controller is presented in [6], where knock probability is maintained under a desired level by updating a map representing the relation between the SA and the expected knock probability.

The main problem with these control strategies is the need of in-cylinder pressure sensor. Despite their high accuracy, in-cylinder pressure sensors, still suffer from cost and durability issues, and also require modifications in the cylinder head to be installed. Although in-cylinder pressure sensors are widely used in the field of engine research, the application on production engines is limited [7, 8].

With the raised computing capacity of electronic control units (ECUs), model-based control has become an interesting tool for difficult applications such as ICE [9]. The combustion process can be modeled by the application of empirical models or by the application of predictive models [10]. In order to replace the use of in-cylinder pressure sensors, different zero-dimensional models have been published in recent years. Such models [11] use maps and empirical coefficients in order to simplify the combustion process and thus reduce calculation time.

Nowadays, alternative fuels are investigated in industry and research communities due to the global warming and rising concerns of fuel security [12, 13]. Gaseous fuels, such as Liquefied Petroleum Gas (LPG) and Compressed Natural Gas (CNG), are used as alternatives to conventional liquid fuels in order to improve emissions [14]. Accordingly, combustion models require to be flexible enough to simulate combustion under different fuels.

Several two-zone combustion models were published in

literature in recent years [15, 16]. These models use a predefined empirical Wiebe function in order to determine the mass-fraction burned rate, which needs to be calibrated for every engine operating condition. A further approximation can be found in [17], where a two-zone real time capable combustion model for SI engines is presented, the model is combined with simplified chemical reaction mechanism being able to predict in-cylinder pressure and thermodynamic properties.

Virtual sensors can be used to improve the estimation of in-cylinder pressure by obtaining information about combustion characteristics, such as ignition delay, peak cylinder pressure and its location. One of the methods in the literature consist on measuring the instantaneous crankshaft speed and extract from this value the information regarding combustion characteristics. In [8] the in-cylinder pressure peak value and its location is estimated through the instantaneous speed measurement. Moreover, in [18] the measurement of the crankshaft speed variation is used to estimate the peak pressure value, peak pressure location, and start of combustion. Further methods use knock sensor signal to obtain information about combustion. For example, in [19] combustion parameters, such as combustion phasing and combustion noise, are computed from a knock sensor. The possibility of identifying the start of combustion and the pressure peak position by real-time processing of the knock sensor signal has been reported in [20]. Additionally, in [8] the 50 % mass fraction burn (CA50) is obtained from knock sensor signal.

These sensors which describe engine dynamics can be integrated with observer structures to estimate the in-cylinder pressure trace, for example by means of sliding mode observers [21, 22], neural networks [23] or Extended Kalman Filter (EKF) [24]. In [25], a model is used to estimate the crankshaft rotation by the estimation of the in-cylinder pressure, which is obtained through the application of Wiebe functions. Furthermore, a EKF method can be found in [26], where an iterative cylinder pressure estimation is proposed, with the engine structure vibration signal as input.

The present work is based on the SI combustion model approach proposed in [27, 28]. This model calculates the amount of burned fuel, which is proportional to the difference between the fuel mass that has entered the flame and the fuel mass that has burned previously, thus representing a mass of fuel that is comprised in a type of flame brush.

In this paper, the combustion model uses knock sensor signal to obtain information about pressure peak location. An Extended Kalman Filter is applied to find the optimal solution between pressure peak location calculated through the model and the measurement from knock sensor. The model is validated in transient condition, comparing the observer results with the measured in-cylinder pressure and the results obtained with the model, showing a useful application to replace in-cylinder pressure sensors. Tests with different fuels are also shown, demonstrating that the observer can adjust the model to different fuels on the same engine.

This article is organized as follows: first, the experimental set-up is described. In the third section the combustion model is presented. Section four shows how to use the information of the knock sensor to update the combustion model by means of an EKF. Results and discussion are shown in section five, and finally, the last section highlights the main benefits of the method presented.

2. Experimental set-up

Two engines, namely engine A and B, have been used to carry out experimental tests:

- Engine A: A four cylinder EURO VI SI production engine fueled with gasoline.
- Engine B: A single-cylinder research version of a 4-stroke turbocharged SI engine fueled with gasoline and CNG.

The main characteristics of the engines and the Research Octane Number (RON) of fuels are shown in Table 1.

Table 1: Engines and fuel specifications

	Engine A	Engine B
Displaced volume	1300 cc	404 cc
Bore (D)	72 mm	80 mm
Stroke	81.2 mm	80.5
Connecting rod length (L_b)	128 mm	133.8 mm
Crank length (L_m)	40.6 mm	40.3 mm
Compression ratio	10.6:1	13:4:1
Combustion type	SI	SI
Injection type	GDI	PFI
Fuel	Gasoline	Gasoline / CNG
RON	95	95/120

The engines were integrated with in-cylinder, intake and exhaust manifold pressure sensors, with a 0.2 crank angle degrees sampling period provided through an optical encoder.

The engines were tested at several operating conditions:

- Training: A total of 80 steady tests, with 500 cycles analyzed at each test, in 11 different operating conditions. The operating conditions tested at training

are shown in Figure 1.

- Validation: Steady and transient tests in similar operating conditions.
  - Steady tests: Four conditions of engine speed were used in engine A, namely 1500, 2000, 2500 and 3000 rpm at 100000 Pa of intake pressure. Engine B was evaluated at a single operating point (4000 RPM and 200000 Pa) using two different fuels in order to evaluated the impact of the calibration.
  - Transient tests: Figure 2 shows the validation transient tests carried out in engine A, where the principal engine variables modified (pedal, engine speed and throttle), and the intake pressure evolution are plotted: $Test_1$ is a load transient with the engine running at 2000 rpm, $Test_2$ is a transient of speed between 1500 and 2000 rpm, and $Test_3$ consist on a sequence of load transients between 80000 Pa and 110000 Pa of intake pressure.

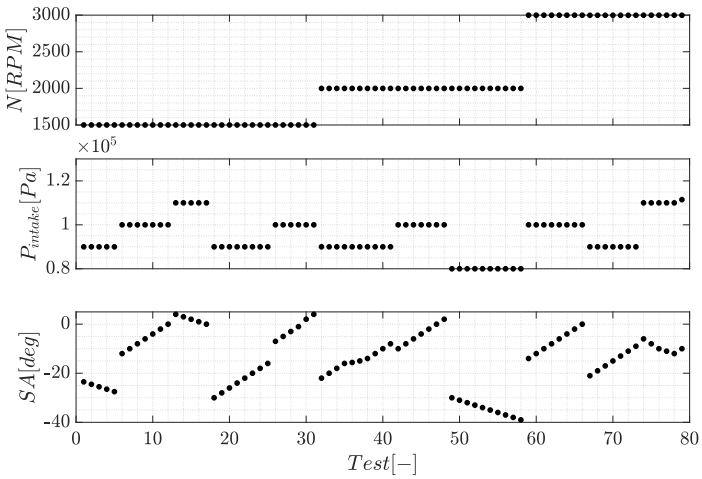

Figure 1: Operating conditions for training tests.

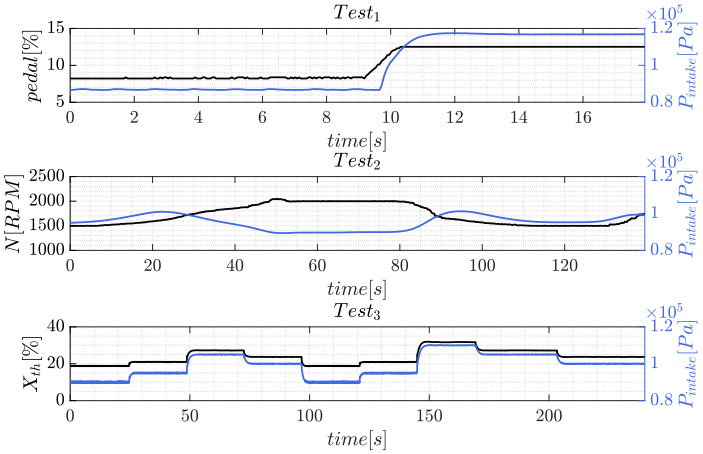

Figure 2: Test performed for validation proposes: pedal position, engine speed (N) and throttle (X_{th}).

3. Combustion model

The combustion has been estimated from a turbulent and laminar combustion model which was originally introduced in [27], and used in [28] to model the cycle to cycle variability of the heat release rate. The main variables and equations of the model are presented in Table 2, while the interested reader is referenced to [28] for a detailed description. A summary of the main equations of the combustion model is shown in Table 2.

The model is based on the assumption of polytropic evolution during the compression stroke, i.e. the in-cylinder pressure (p) can be calculated from its value at the intake valve closing, the volume evolution and the polytropic exponent κ, such as:

$$p = p_{IVC}(\frac{V_{IVC}}{V})^{\kappa} \tag{1}$$

where V is the cylinder volume and IVC subindex represents the intake valve closing.

In this model the start of combustion (SOC) is assumed to be at the SA. When combustion exist, the in-cylinder pressure is computed as:

$$dp = (\frac{\Delta m_b}{14.6} H_c \eta_c - pdV \frac{\kappa}{\kappa - 1}) \frac{\kappa - 1}{V} \tag{2}$$

According to Table 2, the model has three main calibrating variables (X_1, X_2, and X_3): X_1 is related with the laminar speed, while X_2 and X_3 are related with the evolution of the turbulent intensity. The described model considers a flame front evolution by assuming perfect mixture, however, other phenomena, such as stratification effects or residual gases distribution, can be considered by adjusting those parameters. In this work, the model was calibrated for the training conditions tested, and X_1 is adapted using an Extended Kalman Filter and the knock sensor signal as

Table 2: Summary of model equations

Description	Parameter	Equation
Incoming mass	$\frac{\partial m_e}{\partial t}$	$\rho_{ub} A_f (u_t + S_l)$
Burned mass	$\frac{\partial m_b}{\partial t}$	$\frac{m_b - m_e}{\tau} + \rho_{ub} A_f S_l$
Laminar flame speed	S_l	$X_1 S_{l0}(\lambda)(\frac{T_{ub}}{T_0})^{\alpha(\lambda)}(\frac{p}{p_0})^{\beta(\lambda)}(1 - 2.06 RGF^{0.77})$
Flame front area	A_f	$\begin{cases} 2\pi r_b^2 & if \quad r_b \leq h \\ 2\pi r_b^2 h & otherwise \end{cases}$
Turbulent intensity	u_t	$u_{t0} \frac{\rho_{ub}(t)}{\rho_{ub}(SOC)}$
Turbulent intensity at SOC	u_{t0}	$X_2 \overline{up} \sqrt{\frac{\rho(SA)}{\rho(IVC)}}$
Characteristic time	τ	$\frac{\lambda_m}{S_l}$
Mean piston velocity	$\overline{up}$	$2 L_m \frac{n}{60}$
Micro scale length	λ_m	$X_3 \sqrt{\frac{\mu(SA)}{u_{t0}}} \rho_{ub}(SA)^{\frac{1}{3}} (\frac{1}{\rho_{ub}})^{\frac{5}{6}}$
Dynamic viscosity	μ	$3.3 * 10^{-7} T_{ub}^{0.7}$
Adaptation of calibration constant	X_2	$X_{20}(n, p_{intake}) + 0.02 SA$
Chamber height	h	$y_1 + \frac{V_{cc}}{4\pi D^2}$
Piston position throughout the cycle	y_1	$L_b + L_m - L_m cos(\frac{ang\pi}{180}) - \sqrt{L_b^2 - L_m^2 sin(\frac{ang\pi}{180})^2}$
Minimum volume	V_{cc}	$\pi D^2 L_m$

a feedback. X_{20} is obtained through OL tables as shown in [28] while X3 is assumed constant. Table 3 shows a summary of the calibration parameters used in this work.

Table 3: Summary of model constants

Parameter	Description	Value
X_1	Calibration factor	0.5
X_{20}	Calibration factor	OL table
X_3	Calibration factor	10
S_{l0}	for $\lambda = 1$	0.281
α	for $\lambda = 1$	2.129
β	for $\lambda = 1$	-0.217
κ	Adiabatic coefficient	1.3

Finally, the blown down phase is calculated as suggested in [29], where the in-cylinder pressure has linear variation between Exhaust Valve Open (EVO) and Intake Valve Open (IVO) as:

$$p = p_{EVO} + \frac{p_{IVO} - p_{EVO}}{\theta_{IVO} - \theta_{EVO}} (\theta_{IVO} - \theta_{EVO}) \tag{3}$$

where θ represents the crank angle evolution. Notice that the pressure at the intake valve opening (p_{IVO}) is assumed to be the pressure in the intake manifold.

3.1. Residual Gas Fraction estimation

In the model suggested in [28] the RGF is a required input. In this work, the in-cylinder pressure model of the cycle (i) is used to estimate the RGF of the cycle ($i+1$), following:

$$RGF^{i+1} = \frac{m_{res}^i}{m_{cyl}^{i+1}} \tag{4}$$

where m_{res} is the residual gas mass and m_{cyl} the trapped mass. The residual gas mass can be calculated as:

$$m_{res} = \frac{p_{EVC} V_{EVC}}{R T_{exh}} \tag{5}$$

where p_{EVC} and V_{EVC} are the in-cylinder pressure and volume at the exhaust valve closing, R is the gas constant (286 J/Kg.K for the mixture of burned gases and air [30]) and T_{exh} is the exhaust temperature. The cylinder mass in the cycle i can be calculated as:

$$m_{cyl}^i = m_{fuel}^i + m_{air}^i + m_{res}^{i-1} \tag{6}$$

where m_{air} and m_{fuel} are obtained from sensors and models at the ECU.

The exhaust temperature is calculated using polytropic expansion as suggested in [31]:

$$T_{exh} = k_1 p^{\frac{\kappa-1}{\kappa}} \tag{7}$$

where the temperature to pressure ratio k_1 is fitted considering that $T_{exh} = T_{cyl}$ during the end section of the expansion stroke, where T_{cyl} can be estimated from the perfect gas law as:

$$T_{cyl} = \frac{pV}{Rm_{cyl}} \tag{8}$$

For initialization an initial RGF value is assumed ant then it gets updated to fit the aforementioned model.

4. Observer design

The present paper proposes a simple observer design to provide the system with a continuous estimation of the laminar flame speed constant X_1. The aim of the observer is to estimate X_1 by updating a bias in the in-cylinder maximum pressure location.

4.1. In-cylinder peak estimation

As already explained above, the pressure peak in the cylinder can be obtained through different methods, by using the signal from the knock sensor, as suggested in [20]. The method consists on a low pass filter at the knock sensor signal to separate the harmonic components, which is used to find the zero-crossing acceleration angle, that is characteristic of the pressure peak location. In Figure 3 the in-cylinder pressure signal of each cylinder and the filtered knock sensor signal are represented as example.

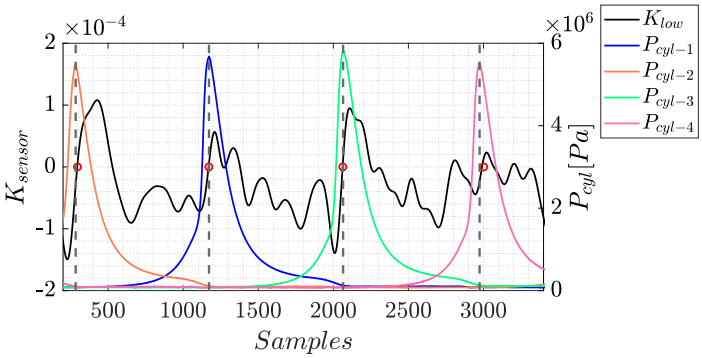

Figure 3: Knock sensor maximum pressure location compared with in-cylinder pressure. 2000 rpm, 950000 Pa intake pressure.

Note that the pressure peak location is significantly correlated to the zero-crossing position of low pass knocking signal K_{low}. Red circles show the zero-crossing angle, which represents the maximum of the pressure peak location obtained through the knock sensor, and in grey dashed line the maximum pressure peak location measurement from in-cylinder pressure signal is also highlighted. Figure 4 (a) shows the histogram of the pressure peak location obtained by both methods, namely in-cylinder pressure P_{loc-p} and knock sensors P_{loc-k}, and Figure 4 (b) the cumulative distribution function over 2000 cycles during $Test_2$.

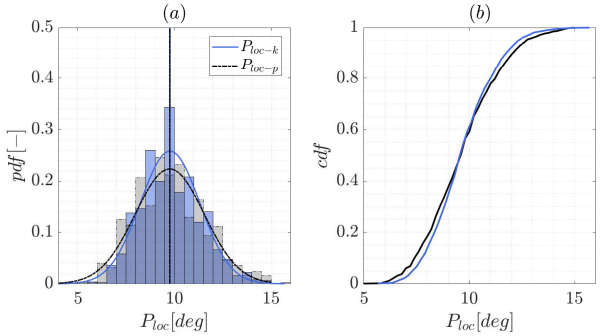

Figure 4: Maximum pressure location obtained from in-cylinder pressure sensor and knock sensor over 2000 cycles (cylinder 2). $R^2 = 0.84$.

As can be seen in Figure 4, the values obtained through the knock sensor are good candidates to estimate the maximum pressure location. In this way and for each cylinder from the knock sensor, cycle by cycle, a feedback of the pressure peak location is used to develop an observer.

4.2. Observer: Extended Kalman Filter

The Kalman Filter is a data fusion technique aimed to combine information from different sources (i.e. model and sensor) to provide the best estimation of a given vabiable. The Kalman Filter is the optimal estimator in the case of gaussian noise in both model and sensor signals [32]. In the case at hand, an Extended Kalman Filter is applied to estimate the proper value of the calibration constant X_1 in a cycle-by-cycle basis to minimize the discrepancies of the model and the knock sensor in the estimation of the angle for the peak pressure. An Extended Kalman Filter (EKF) was designed with one cycle step, since the model is not linear, and an state space system is required. The state space representation of the system is:

$$x_{k+1} = x_k + w_k \tag{9}$$

$$y_k = f(u, x_k) + v_k \tag{10}$$

where, in this case, the sate (x) is the calibration constant of the laminar flame speed (X_1), y are the outputs of the

combustion model measured, i.e. the peak pressure location, u the inputs of the combustion model, v the noise associated to the outputs of the model, and v the noise associated to the states equation.

$$\begin{array}{rcl} x & = & X_1 \\ y & = & P_{loc} \end{array} \tag{11}$$

The state vector of the EKF is defined as follows:

$$\begin{array}{rcl} \hat{x}_{k|k-1} & = & \hat{x}_k \\ e_k & = & y_k - f(u_k, \hat{x}_{k|k-1}) \\ \hat{x}_k & = & \hat{x}_{k|k-1} + K_k e_k \end{array} \tag{12}$$

The Kalman gain value (K) is updated as:

$$\begin{array}{rcl} P_{k|k-1} & = & F_k P_{k-1} F_k^T + W_k \\ K_k & = & P_{k|k-1} H_k^T (H_k P_{k|k-1} H_k^T + R_k)^{-1} \\ P_k & = & (I - K_k H_k) P_{k|k-1} \end{array} \tag{13}$$

where w and v are modeled as a Gaussian distribution with zero mean and co-variance matrices W_k and R_k. The linear state matrices, F_k and H_k, represents Eqs. (9) and (10). Because these equations are non-linear an Extended Kalman Filter (EKF) was used by linearising them, as following:

$$H_k = \frac{d(f(u, x_k))}{dx_k} = \frac{f(u, x_k) - f(u, x_k + \Delta_{x_k})}{\Delta_{x_k}} \tag{14}$$

The scheme of the complete combustion model proposed in this work (EKF model) is shown in Figure 5. The knock sensor signal (K_{signal}) is used to estimate the pressure peak location (P_{loc-k}) and it is used in the EKF to update the state X_1 by using the combustion model. The final pressure signal obtained can be used to extract information from the complete combustion, such as CA10, CA50, CA90, IMEP, or RGF.

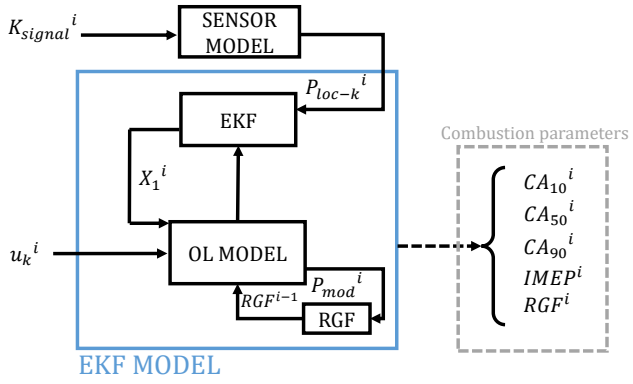

Figure 5: EKF model scheme proposed.

Note that as already mentioned above, the RGF is obtained cycle by cycle from the pressure of the model (P_{mod}), and used in the following cycle as input (RGF^{i+1}).

The noise of each variable characterize the performance of the EKF, low noises associated to the measured signal exhibit a fast adaptation, while low noises associated to the model become in a more smooth but filtered signal at the output. Figure 6 shows the pressure peak location obtained through EKF model (in black), and two possible combination of v and w (Noise A and Noise B), used during $Test_2$. Noise A (in blue) is the output of the model when the values collected in Table 4 are used, and Noise B (in grey) show the effect of considering a lower noise at the model prediction of X_1.

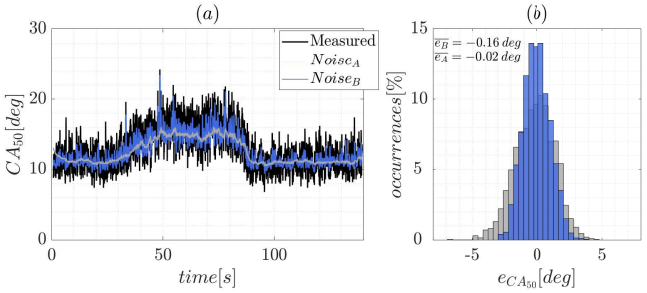

Figure 6: Model results applying a Kalman filter at a speed transient in Cylinder 2. Left plot (a): CA50 evolution. Right plot(b): Absolute error histogram at the CA50 for Noises A and B.

Table 4: Noise suggested for Kalman filter

Variable	Type	Value [unit]
X_1	state	0.005 [-]
P_{loc}	output	1[deg]

Applying the values collected in Table 4 at different engine speeds, the results of Figure 7 are obtained. Here, the histogram of the absolute error for four engine speeds is shown with the engine running at 100000 Pa of intake pressure.

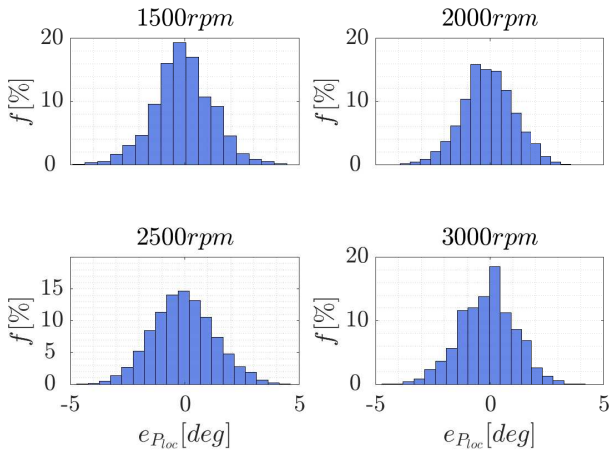

Figure 7: Absolute error histograms at different rpm at 100000 Pa intake pressure. Cylinder 2.

In Figure 8 the EKF model is applied in steady state condition for different X_1 initial values. In (a) the X_1 value is shown, and in (b) the output of the model and the measured value P_{loc} are plotted, note that regardless of the initial value , the method converges to the same value in between 2 and 5 seconds independently on the initial conditions. The plot shows the results from cylinder 2 as example.

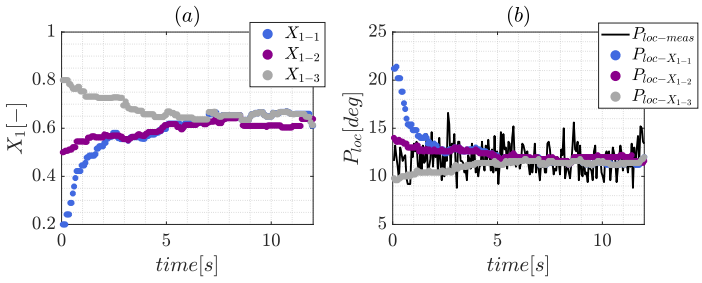

Figure 8: X_1 results for different initial conditions.

5. Results and discussion

In this section results obtained through the EKF model are compared with the results of the OL model, representing the model with constant X_1 and RGF.

Figure 9 shows the state X_1 during the load transient test ($Test_1$) for each one of the four cylinders.

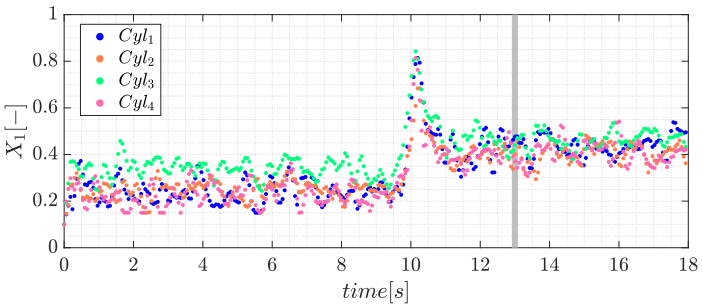

Figure 9: X_1 value during $Test_1$

The in-cylinder pressure evolution at $t = 13s$ (highlighted in gray line) of each cylinder is represented in Figure 10. In black the real in-cylinder pressure (p_{real}), in blue the pressure obtained through the EKF model (p_{EKF}), and in gray the model obtained without feedback information (p_{OL}).

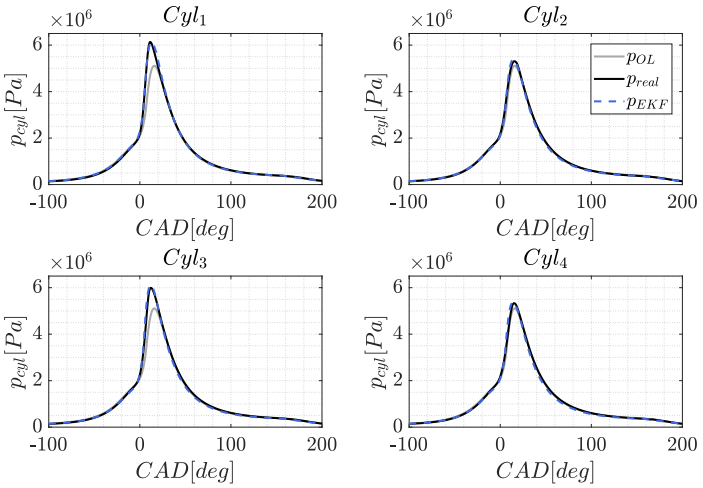

Figure 10: In-cylinder pressure evolution measured compared with EKF and OL models during $Test_1$ cycle labeled in figure 8.

As can be seen in Figure 10, the model proposed is able to adapt the parameters according to the feedback of each cylinder signal, the result of this adaption is a better representation of the evolution of the in-cylinder pressure than with the use of only open loop tables .

In Figure 11 the pressure peak location for both models, EKF and OL, are compared with the pressure peak location measured by the in-cylinder pressure sensors of each cylinder.

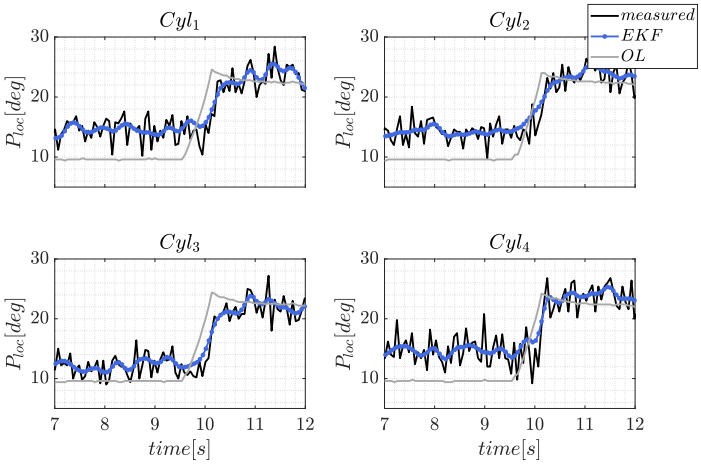

Figure 11: In-cylinder pressure measured compared with EKF and OL models during $Test_1$ cycle labeled in figure 8.

As can be seen in Figure 11, in the case of the OL model output of is always the same since the inputs (cycle operating conditions) are the equal for all cylinders. On the other hand, in the case of the EKF model, the output from each cylinder is different, being able to better represent the each cylinder.

In Figure 12 on the left side the error histogram for the pressure peak location ($e_{P_{loc}}$) and on the right side the error histogram for one of the combustion parameters CA10 ($e_{CA_{10}}$) are shown, starting from top to bottom the cylinders from one to four are represented. In black the mean error is marked, in dashed line for the model proposed ($\overline{e_{EKF}}$) and in continuous line the error from open loop model ($\overline{e_{OL}}$).

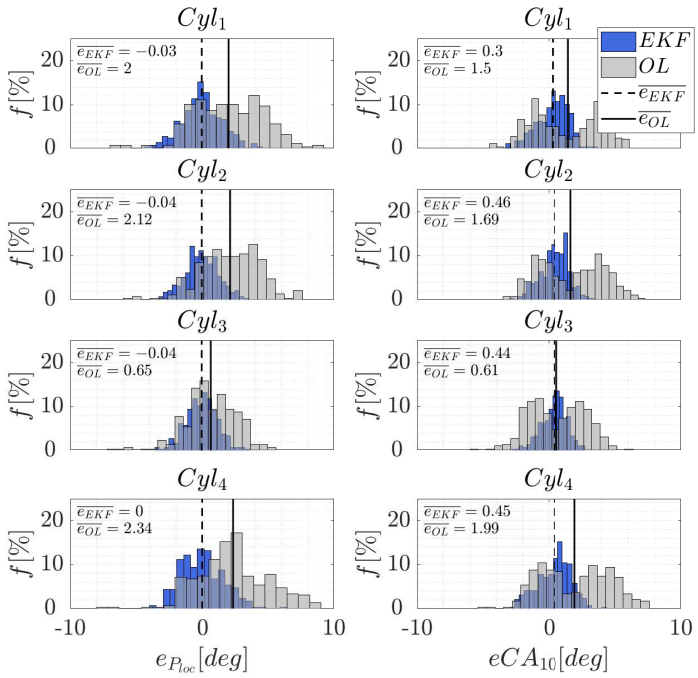

Figure 12: Error histogram for $Test_1$. Left plots: Absolute error for P_{loc}. Right plot: Absolute error for CA10.

As can be seen in Figure 12, the mean error for both parameters at all cylinders obtained from $Test_1$ is around zero. On the other hand, as the OL model uses the same parameters for all the cylinders, the error in the estimation for each cylinder is noticeably different since the result of the model is the same for all cylinders, being cylinder 3 the one with the lowest mean error and cylinder 4 with higher mean error.

In order to compare both models on a single cylinder, different combustion parameters have been extracted, such as CA10, CA50, CA90, IMEP and RGF and compared with the value obtained from the in-cylinder pressure. In Figure 13 the results calculated from the proposed model (color blue) are compared with the results obtained through the open loop model (color gray) and with the measurement from the in-cylinder pressure (color black) during $Test_3$ in cylinder 3.

As can be seen in Figure 13, not only the estimation through the EKF model shows an improvement on the location of the combustion (P_{loc}), but an improvement in the estimation of the CA_x, IMEP and RGF is observed. The error histograms of the variables represented in Figure 13 are shown in Figure 14. Here the values of both methods, compared with the obtained from in-cylinder pressure, are plotted.

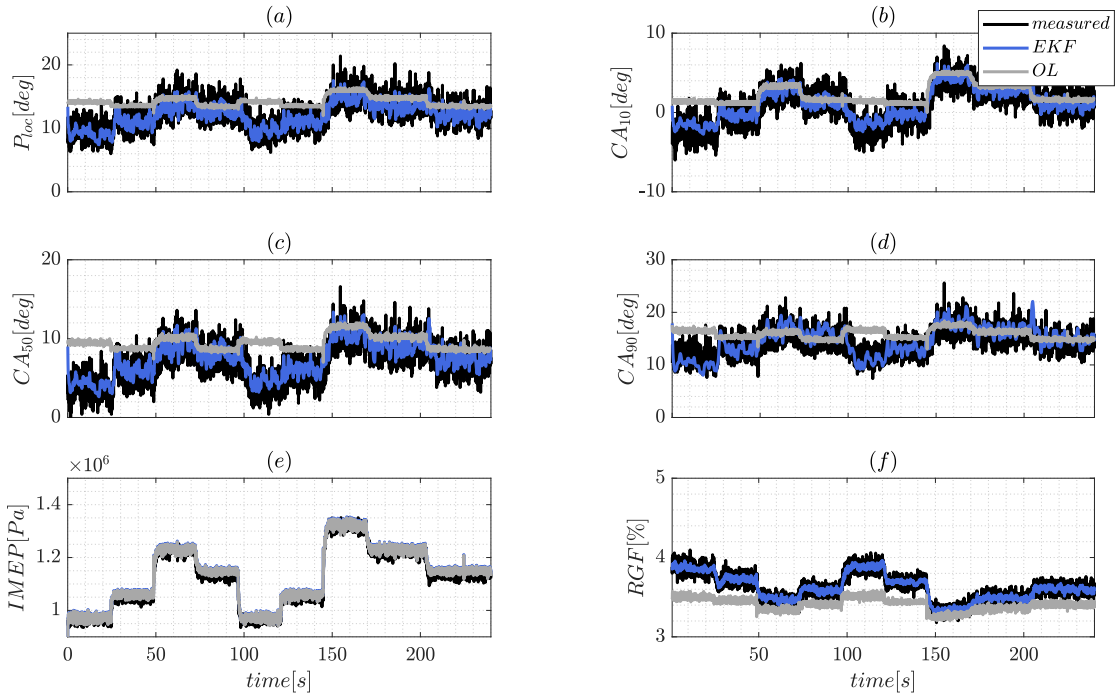

Figure 13: Model results compared with measured value for $Test_3$ for cylinder 3. (a) : pressure peak location, (b) : CA10 (c) : CA50, (d): CA90, (e): IMEP and (f): RGF.

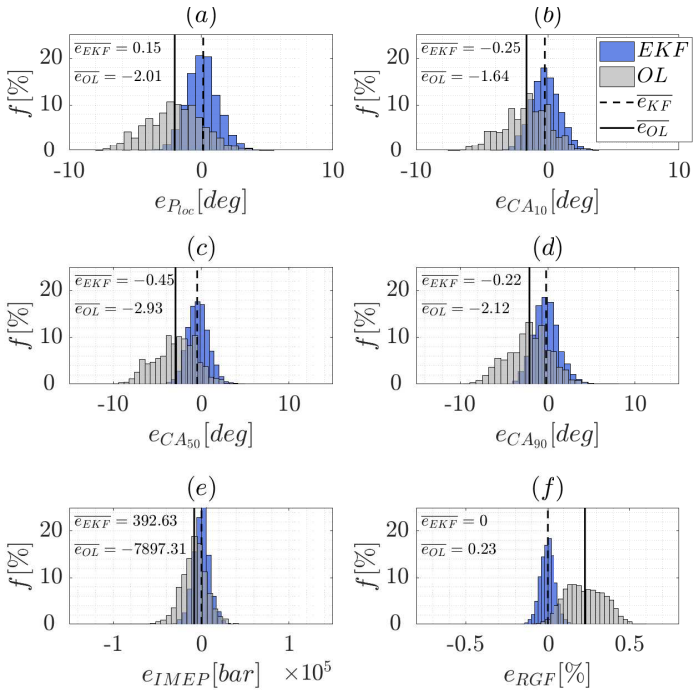

Figure 14: Error histograms for EKF model and OL model. (a) : pressure peak location, (b) : CA10, (c) : CA50, (d): CA90, (e): IMEP and (f)

Analyzing Figure 14, not only the mean error obtained through EKF model is lower than in the case of OL model, but the maximum error obtained is also lower, showing an improvement for the approximation of combustion parameters.

Table 5 summarize the mean relative error between the measurement and the model, during $Test_3$ for the different combustion variables for all cylinders.

Table 5: Mean relative error of EKF model combustion parameters for the four cylinders during $Test_3$.

	Cyl_1	Cyl_2	Cyl_3	Cyl_4
$Variable$	$MRE[\%]$	$MRE[\%]$	$MRE[\%]$	$MRE[\%]$
P_{loc}	7.46	5.84	8.26	7.29
CA10	6.3	6.1	7.56	6.85
CA50	7.5	5.7	8.66	7.8
CA90	8.9	9.12	8.47	9.05
IMEP	1.1	0.82	0.64	2.1
RGF	1.2	1.1	0.96	1.06

Open loop model cannot precisely represent the combustion evolution during transient tests because is restricted to a constant X_1, which was previously calibrated with the training data set in steady conditions (Figure 1). Oppositely, the EKF allows a model adaptation with X_1 as the main degree of freedom to better adjust the output of the observer.

5.1. Fuel impact

The fuel impact is analyzed in engine B for a given steady operating condition. In Figure 15, the fitted cali-

bration constant X_1 over 200 cycles is shown for two cases: gasoline and CNG.

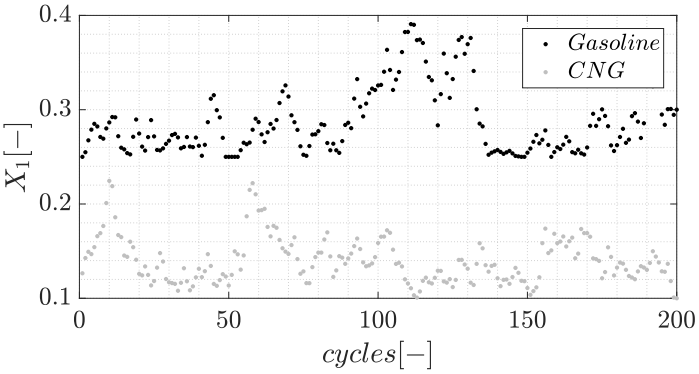

Figure 15: X_1 value for steady test performed in engine B for two cases: gasoline and CNG.

Analyzing Figure 15, the laminar flame speed is lower for cycles fueled with CNG, which experimental studies shows that at equal equivalence ratio the laminar flame speed is smaller for CNG than gasoline [33].

In Figure 16, the in-cylinder pressure evolution for all cycles is shown, in black line the mean value is represented and in blue dashed line the model result.

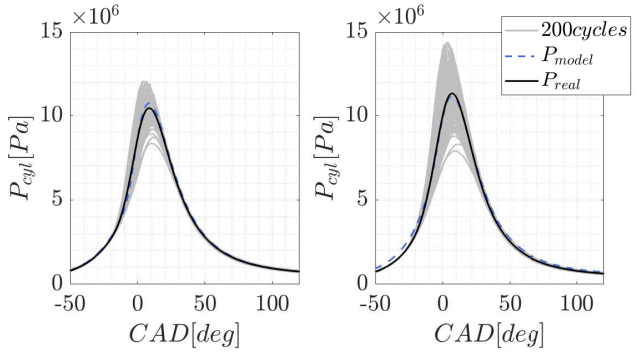

Figure 16: In-cylinder pressure over 200 cycles: Gasoline (left) and CNG (right)

As can be seen in Figures 15 and 16, the model is able to reproduce in-cylinder pressure for different fuel types, by updating X_1 value.

6. Conclusions

An observer has been designed to update a two-phase 0D combustion model with a measurement of the knock sensor signal. A calibration parameter of the model is updated cycle to cycle using an Extended Kalman Filter. It has been demonstrated that the adaptation of the model is not only an improvement for the estimation of different combustion parameters, but also provides more reliable information to analyze the operation of the different cylinders, to adjust to different types of fuels and injection settings. The model proposed was validated in three transient conditions, where the engine speed, pedal position and throttle were modified, ensuring a continuous estimation of the pressure peak location, CA_{10}, CA_{50}, CA_{90}, RGF and IMEP. The model is able to reproduce the combustion parameters with a mean relative error bellow 10 %.

The model can be used in on-line applications to improve the performance of controllers. Future work is devoted to implement in real time the presented combustion model to control variables such as spark advance or variable valve timing.

7. Acknowledgments

Irina A. Jimenez received a funding through the grant 132GRISOLIAP/2018/132 from the Generalitat Valenciana and the European Social Fund.

References

[1] Q. Xin, Diesel engine system design, Elsevier, 2011.
[2] D. Neumann, C. Jörg, N. Peschke, J. Schaub, T. Schnorbus, Real-time capable simulation of diesel combustion processes for hil applications, International Journal of Engine Research 19 (2) (2018) 214–229.
[3] E. Pipitone, A comparison between combustion phase indicators for optimal spark timing, Journal of engineering for gas turbines and power 130 (5) (2008).
[4] E. Corti, C. Forte, G. Mancini, D. Moro, Automatic combustion phase calibration with extremum seeking approach, Journal of Engineering for Gas Turbines and Power 136 (9) (2014).
[5] Y. Zhang, T. Shen, On-board map learning-based combustion phase control in spark ignition engines, in: 2017 IEEE Conference on Control Technology and Applications (CCTA), IEEE, 2017, pp. 287–292.
[6] B. n Pla, P. Bares, I. Jiménez, C. Guardiola, Y. Zhang, T. Shen, A fuzzy logic map-based knock control for spark ignition engines, Applied Energy 280 (2020) 116036.
[7] D. Siano, D. D'agostino, Knock detection in si engines by using the discrete wavelet transform of the engine block vibrational signals, Energy Procedia 81 (2015) 673–688.
[8] F. Taglialatela, N. Cesario, M. Porto, S. Merola, P. Sementa, B. Vaglieco, Use of accelerometers for spark advance control of si engines, SAE International Journal of Engines 2 (1) (2009) 971–981.
[9] R. Finesso, G. Hardy, A. Mancarella, O. Marello, A. Mittica, E. Spessa, Real-time simulation of torque and nitrogen oxide emissions in an 11.0 l heavy-duty diesel engine for model-based combustion control, Energies 12 (3) (2019) 460.
[10] M. Sjerić, D. Kozarac, H. Schuemie, R. Tatschl, A new quasi-dimensional flame tracking combustion model for spark ignition engines, Energy Conversion and Management 165 (2018) 263–275.
[11] S. Verhelst, C. Sheppard, Multi-zone thermodynamic modelling of spark-ignition engine combustion–an overview, Energy Conversion and Management 50 (5) (2009) 1326–1335.
[12] Q. Tang, X. Duan, Y. Liu, S. Li, Z. Zhao, K. Ren, Y. Li, H. Chang, Experimental study the effects of acetone–butanol–ethanol (abe), spark timing and lambda on the performance

and emissions characteristics of a high-speed si engine, Fuel 279 (2020) 118499.
[13] R. Daniel, G. Tian, H. Xu, S. Shuai, Ignition timing sensitivities of oxygenated biofuels compared to gasoline in a direct-injection si engine, Fuel 99 (2012) 72–82.
[14] P. Napolitano, M. Alfè, C. Guido, V. Gargiulo, V. Fraioli, C. Beatrice, Particle emissions from a hd si gas engine fueled with lpg and cng, Fuel 269 (2020) 117439.
[15] A. Ibrahim, S. Bari, A comparison between egr and lean-burn strategies employed in a natural gas si engine using a two-zone combustion model, Energy Conversion and Management 50 (12) (2009) 3129–3139.
[16] M. S. Lounici, K. Loubar, M. Balistrou, M. Tazerout, Investigation on heat transfer evaluation for a more efficient two-zone combustion model in the case of natural gas si engines, Applied Thermal Engineering 31 (2-3) (2011) 319–328.
[17] R. C. Li, G. G. Zhu, A control-oriented reaction-based si engine combustion model, in: Dynamic Systems and Control Conference, Vol. 51906, American Society of Mechanical Engineers, 2018, p. V002T27A002.
[18] F. Mocanu, D. Taraza, Estimation of main combustion parameters from the measured instantaneous crankshaft speed, Tech. rep., SAE Technical Paper (2013).
[19] J. Chauvin, O. Grondin, E. Nguyen, F. Guillemin, Real-time combustion parameters estimation for hcci-diesel engine based on knock sensor measurement, IFAC Proceedings Volumes 41 (2) (2008) 8501–8507.
[20] A. Businaro, N. Cavina, E. Corti, G. Mancini, D. Moro, F. Ponti, V. Ravaglioli, Accelerometer based methodology for combustion parameters estimation, Energy Procedia 81 (2015) 950–959.
[21] I. Haskara, L. Mianzo, Real-time cylinder pressure and indicated torque estimation via second order sliding modes, in: Proceedings of the 2001 American Control Conference.(Cat. No. 01CH37148), Vol. 5, IEEE, 2001, pp. 3324–3328.
[22] A. Al-Durra, Adaptive sliding mode observer for engine cylinder pressure imbalance under different parameter uncertainties, IEEE Access 2 (2014) 1085–1091.
[23] S. Trimby, J. F. Dunne, C. Bennett, D. Richardson, Unified approach to engine cylinder pressure reconstruction using time-delay neural networks with crank kinematics or block vibration measurements, International Journal of Engine Research 18 (3) (2017) 256–272.
[24] Q. Wang, T. Sun, Z. Lyu, D. Gao, A virtual in-cylinder pressure sensor based on ekf and frequency-amplitude-modulation fourier-series method, Sensors 19 (14) (2019) 3122.
[25] A. Al-Durra, M. Canova, S. Yurkovich, A real-time pressure estimation algorithm for closed-loop combustion control, Mechanical Systems and Signal Processing 38 (2) (2013) 411–427.
[26] R. Han, C. Bohn, G. Bauer, Recursive engine in-cylinder pressure estimation using kalman filter and structural vibration signal, IFAC-PapersOnLine 51 (31) (2018) 700–705.
[27] N. C. Blizard, J. C. Keck, Experimental and theoretical investigation of turbulent burning model for internal combustion engines, SAE Transactions (1974) 846–864.
[28] B. Pla, J. De la Morena, P. Bares, I. Jiménez, Cycle-to-cycle combustion variability modelling in spark ignited engines for control purposes, International Journal of Engine Research (2019) 1468087419885754.
[29] H. Shen, J. Zhang, B. Yang, B. Jia, Development of a marine twostroke diesel engine mvem with incylinder pressure trace predictive capability and a novel compressor model, Journal of Marine Science and Engineering 8 (3) (2020) 204.
[30] M. Lapuerta, O. Armas, J. Hernández, Diagnosis of di diesel combustion from in-cylinder pressure signal by estimation of mean thermodynamic properties of the gas, Applied Thermal Engineering 19 (5) (1999) 513–529.
[31] C. Guardiola, P. Olmeda, B. Pla, P. Bares, In-cylinder pressure based model for exhaust temperature estimation in internal combustion engines, Applied Thermal Engineering 115 (2017) 212–220.
[32] C. Guardiola, B. Pla, P. Bares, A. Stefanopoulou, Cylinder charge composition observation based on in-cylinder pressure measurement, Measurement 131 (2019) 559–568.
[33] L. Ben, G. Charnay, R. Truquet, Influence of air/ fuel ratio on cyclic variation and exhaust emission in natural gas si engine. sae paper 992901, 1999.